PCCP

PAPER

Cite this: *Phys. Chem. Chem. Phys.*, 2018, **20**, 7570

Electrochemical nanoarchitectonics through polyaminobenzylamine–dodecyl phosphate complexes: redox activity and mesoscopic organization in self-assembled nanofilms†

Agustín Lorenzo,[a] Waldemar A. Marmisollé,*[a] Eliana M. Maza,[ab] Marcelo Ceolín[a] and Omar Azzaroni[a]

Received 4th December 2017,
Accepted 11th February 2018

DOI: 10.1039/c7cp08139a

rsc.li/pccp

Molecular design and preparation of redox active films displaying mesoscopic levels of organization represents one of the most actively pursued research areas in nanochemistry. These mesostructured materials are not only of great interest at the fundamental level because of their unique properties but they can also be employed for a wide range of applications such as electrocatalysts, electronic devices, and electrochemical energy conversion and storage. Herein, we introduce a simple and straightforward strategy to chemically modify electrode surfaces with self-assembled electroactive polyelectrolyte–surfactant complexes. These assemblies are composed of amino-appended polyaniline and monododecyl phosphate. The complexes were deposited by spin-coating and the films were characterized by spectroscopic and X-ray-based techniques: XRR, GISAXS, WAXS, and XPS. The films presented a well-defined lamellar structure, directed by the strong interaction between the phosphate groups and the positively charged amine groups in the polyelectrolyte. These films also displayed intrinsic electroactivity in both acidic and neutral solutions, showing that the polymer remains electroactive and ionic transport is still possible through the stratified and hydrophobic coatings. The stability and enhanced electroactivity in neutral solutions make these assembled films promising building blocks for the construction of nanostructured electrochemical platforms.

Introduction

The use of ionic self-assembled polyelectrolyte–surfactant complexes in the solid state is a systematic and flexible strategy to prepare composites having interesting properties emerging from the combination of the functionalities of individual blocks.[1,2] These systems are known to be good examples of bottom-up synthetic routes for the construction of complex hybrid interfaces and constitute emblematic examples of the emerging field of nanoarchitectonics.[3–6] Inside these architectures, the polyelectrolytes provide mechanical stability whereas the surfactants provide their capacity to form highly ordered mesophases. The modular formation of polyelectrolyte–surfactant complexes is versatile because of the myriad of commercially available building blocks. Among many kinds of different polyelectrolytes that can be used to form the complexes organic conducting polymers emerge as specially interesting combining structural and electrical properties.[7–9] The casting of thin films formed by conducting polyelectrolytes and surfactants offers the opportunity to produce a variety of new electroactive materials with interesting properties such as self-order and non-wetting characteristics,[10] becoming a versatile material system that contributes to the development of the thriving field of electrochemical nanoarchitectonics.[11,12]

Among others, polyaniline (PANI) has been one of the most popular conducting polyelectrolytes because of its low cost and ease of synthesis,[13,14] making PANI-based materials promising building blocks in the construction of electroactive complex interfaces for applications from biosensing to energy storage.[15] Although some intrinsic mesoscopic ordering has been reported for the deposition of PANI on solid substrates under specific conditions,[16,17] a systematic way to produce meso-organization is to employ surfactants as structure-directors with some examples of surfactant-induced PANI mesostructures.[18,19]

The usual strategy to form mesostructured films from polyelectrolytes and surfactants consists of dissolving each component separately (usually in aqueous solutions), then

[a] *Instituto de Investigaciones Fisicoquímica Teóricas y Aplicadas (INIFTA), Departamento de Química, Facultad de Ciencias Exactas, Universidad Nacional de La Plata (UNLP), CONICET, 64 and 113, La Plata, Argentina. E-mail: wmarmi@inifta.unlp.edu.ar*

[b] *Soft Matter Nanotechnology Group, CIC biomaGUNE, Paseo Miramón 182, 20009 San Sebastián, Gipuzkoa, Spain*

† Electronic supplementary information (ESI) available: Additional spectroscopic and electrochemical results. See DOI: 10.1039/c7cp08139a

co-precipitating the electrostatic complex by mixing, re-dissolving the hydrophobic precipitate in a suitable organic solvent and finally depositing the surfactant–polyelectrolyte complex on solid surfaces by spin-coating or drop-casting. Although chemical synthesis of PANI is simple and well-known, its subsequent processability in aqueous dispersions poses complex challenges.[20] For this reason, PANI oligomers have been proposed as an alternative material due to their higher solubility. The self-assembly of PANI oligomers with bulky surfactants has been reported.[21,22] Moreover, depending on casting conditions, films with different well-defined structures can be achieved.[21,22] However, we have recently reported the chemical synthesis of polyaniline having pendant additional amino groups from the oxidative polymerization of 3-aminobenzylamine (PABA).[23] This electroactive polymer presents higher solubility in acidic solutions, making it possible to use its dispersions for layer-by-layer assembly with polyanions. Additionally, PABA also displays enhanced electroactivity in neutral solutions compared with PANI.[23,24] Owing to its improved processability in aqueous solution, PABA seems to be a better candidate than PANI for the preparation of electrostatically-driven complexes with surfactants.

On the other hand, the particular interaction between protonated amines and phosphate anions has been extensively recognized. The association of amines and phosphate anions plays a key role in the self-assembly of multiple biological supramolecular structures, such as the aggregates of proteins in biosilica,[25,26] and the nuclear aggregates of polyamines in many replicating cells.[27,28] Recently, it has been demonstrated that the aggregation of polyallylamine hydrochloride (PAH) and phosphates from solution can be used for the reversible modification of different substrates.[29] NMR studies indicate that electrostatic interactions between PAH and phosphates are present in the whole pH range in which amines are protonated. Moreover, phosphates produce aggregates more efficiently than other polyvalent anions and it has even been suggested that protonated amines induce an additional dissociation of phosphate anions.[30] Recently, we have shown that phosphate anions interact much more strongly with charged amines than similar divalent anions, due to the effectiveness of hydrogen bonding interactions, and this association induces both a higher protonation degree of amines and a higher dissociation degree of phosphates.[31]

In this work, we present a simple method to obtain self-assembled electroactive nanofilms formed by polyaminobenzylamines (PABA) and sodium monododecyl phosphate (DP) by combining the specific amine-phosphate supramolecular interaction with the structural driving force of the polyelectrolyte–surfactant complexation. By a particular interplay of interactions, it is possible to obtain both a well-defined lamellar structure and good electroactivity in neutral solutions, which make these nanofilms promising platforms for the construction of functional bioelectrochemical devices.

Experimental

Chemicals

Ammonium persulfate (APS, 98%), 3-aminobenzylamine (ABA, 99%), and sodium monododecyl phosphate (DP, 98%) were purchased from Sigma Aldrich. HCl, KCl and sulfuric acid were purchased from Anedra. All chemicals were of analytical or reagent grade and they were utilized without further purification. All solutions were prepared with Milli-Q water (18.2 MΩ cm).

PABA synthesis

Poly(3-aminobenzylamine) (PABA) was synthesized through the chemical oxidation of ABA with APS.[23] Briefly, a 10 mM ABA solution was prepared in water. Then, solid APS was added to form a 10 mM solution. After 1 hour of continuous stirring, the pH was shifted to 10 by adding 10% KOH. Then, the solution was centrifuged and the precipitate was re-dispersed in 0.5 M HCl up to the same initial volume.

Preparation of the assembled films

A 20 mM solution of DP was prepared in 0.5 HCl. The complexes PABA–DP were prepared by mixing the PABA and DP solutions in different proportions. The ratios of PABA : DP chosen were 1 : 2, 1 : 5 and 1 : 10, where the surfactant was always in excess. The dispersions formed a precipitate and were centrifuged at 7000 rpm and the supernatant was discarded. The precipitates were kept overnight under a vacuum at 45 °C. The dry-solid product was dissolved again in 400 μL of DMF and spin-coated onto Au or Si(100) substrates for thin film assembly. All the films, independently of the amount of sample and the substrate used, were prepared under the same spin-coating program. The entire film preparation procedure is depicted in Scheme 1.

Film characterization

Fourier transform infrared spectroscopy in the attenuated total reflection mode (ATR-FTIR) was performed using a Varian 600 FTIR spectrometer equipped with a ZnSe ATR crystal with a resolution of 4 cm^{-1}.

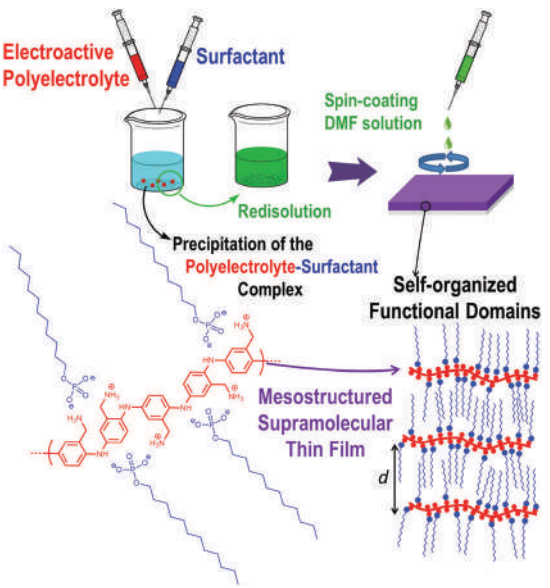

Scheme 1 Representation of the preparation procedure and structure of the films.

Atomic force microscopy (AFM) was performed with a Veeco Multimode AFM connected to a Nanoscope V controller which was used to image the substrate. AFM measurements were performed in tapping mode in air using a TESP-V2 (Bruker, K = 42 N m^{-1}) cantilever.

Contact angles were measured using a Ramé-Hart contact angle system (Model 290). The average contact angle value was obtained by dispensing 1 μL-droplets of Milli-Q water at five different positions on the film-modified substrates.

Cyclic voltammetry (CV) was performed using a Gamry REF600 potentiostat. Gold electrodes were prepared by sputtering on glass substrates utilizing a thin layer of Ti to improve the adhesion. The electrochemical cell was a three electrode Teflon cell with a 2 mL volume capacity. The Au working electrodes were sealed with an o-ring defining an electroactive area of 0.145 cm^2. The counter electrode was a Pt wire, and a Ag/AgCl (3 M NaCl) electrode was utilized as a reference.

X-ray characterization

X-Ray photoelectron spectroscopy (XPS) was performed using a SPECS SAGE HR 100 system spectrometer. A Mg Kα (1253.6 eV) X-Ray source was utilized operating at 12.5 kV and 10 mA. The take-off angle was 90° and the operating pressure was 8 × 10^{-8} mbar. Quantitative analysis of the spectra was carried out by using Casa XPS 2.3. 16 PR 1.6 software, using Shirley baselines and Gaussian\Lorentzian (30%) product functions. To compensate for surface-charging effects, the binding energy (BE) of the aliphatic core level C1s was set at 285 eV.[29] The full width at half maximum (FWHM), was kept fixed for different components of a given element. For N/P, more precise calculations were performed by recording the XPS spectrum $(NH_4)_2HPO_4$ (Sigma Aldrich) powder under the same conditions as an internal reference.

X-Ray Reflectivity (XRR) and Grazing-Incidence Small-Angle X-Ray Scattering (GISAXS) measurements were performed at the D10A-XRD2 line of Laboratório Nacional de Luz Síncrotron (LNLS, Campinas, Brazil). A monochromatic beam of 7709 eV (λ = 1.608 Å) and a sample-to-detector distance of 600 mm were used to perform the experiments.

Wide Angle X-Ray Scattering (WAXS) measurements were carried out using a XEUSS 1.0 HR (XENOCS, Grenoble) installed at INIFTA (La Plata, Argentina) (project "Nanopymes", EuropeAid/132184/D/SUP/ARContract 331-896). The equipment has a microfocus X-ray source and a Pilatus 100K detector (Dectris, Switzerland).

Results and discussion

XPS

Chemical characterization of the self-assembled films was performed using XPS. The spectra in the N1s core region were determined for PABA (drop-casted from acidic aqueous solution) and the assembled films with DP onto Au. The N1s core spectrum level of PABA can be deconvoluted into 5 peaks as previously reported.[23,24] The backbone N atoms are considered to contribute

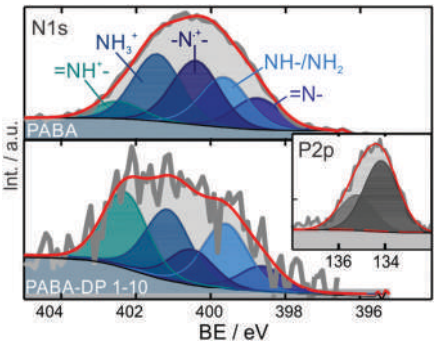

Fig. 1 N1s XPS spectra of PABA (top) and PABA–DP 1 : 10 (bottom) films deposited on Au. Grey lines are experimental spectra; red lines mean the global fittings. Chemical assignments for each component are presented in the plot. Inset: P2p XPS signal for the assembled film.

with 4 bands corresponding to the uncharged N species and positive N species from oxidized secondary amines and protonated imine (Fig. 1). The N1s core spectra of the films presented similar characteristics. Detailed assignments and proportion of the different N species are presented as ESI.† For the three films studied, the proportion of positively charged quinone-like moieties increases if compared with PABA (Fig. 1), suggesting that the interaction with DP stabilizes this oxidized form. As it was reported for the LbL assembly of PABA with polyanions,[23] the increment in the proportion of oxidized forms of N (polaron and imine structures, BE > 400 eV) when interacting with the surfactant in the films suggests that the DP could also act as a dopant improving its electroactivity.[32,33]

Quantitative composition analysis was performed studying the P2p core region of the XPS spectra (Fig. 1). The XPS spectrum of diammonium hydrogen phosphate was used as a reference to obtain the correct relative cross sections of nitrogen and phosphorus. No significant differences were obtained in the composition of the films assembled from solutions with different initial proportions of DP (Table 1). Furthermore, when considering just the positive nitrogen forms (BE > 400 eV, see the ESI†), the values of the ratio of positive N to phosphate are 1.0, 0.9 and 1.1 for 1 : 10, 1 : 5 and 1 : 2 PABA–DP films respectively. This is consistent with an intrinsic charge compensation mechanism within the films; *i.e.* the positive charges on the PABA chains are compensated and stabilized by interaction with the negatively charged phosphate groups of the surfactant (assumed to be singly charged due to the acidic pH of the assembling conditions for the preparation of the PABA–DP complexes).

Summing up, our XPS results confirm that the self-assembled films are stabilized by electrostatic interactions between the positive charged amine groups of PABA and the negative charged groups of DP.

ATR-FTIR

The self-assembled films were further characterized using ATR-FTIR. The ATR-FTIR spectra of PABA, DP and self-assembled films on gold substrates are shown in Fig. 2. Spectra of the films were not rescaled, so the different intensities are due to the

Table 1 Summary of some features for the PABA–DP self-assembled films

Sample	Thickness[a] (nm)	$\nu_{CH_2,asym}$[b] (cm^{-1})	(Asym/sym) ratio[b]	N/P ratio[c]	Contact angle (°)
DP	—	2916	1.5	—	—
PABA–DP 1 : 10	34	2922	2.7	1.5	107
PABA–DP 1 : 5	22	2924	3.1	1.4	102
PABA–DP 1 : 2	10	2927	3.6	1.3	85

[a] Determined by ellipsometry (ESI). [b] From the FTIR spectra. [c] From XPS analysis.

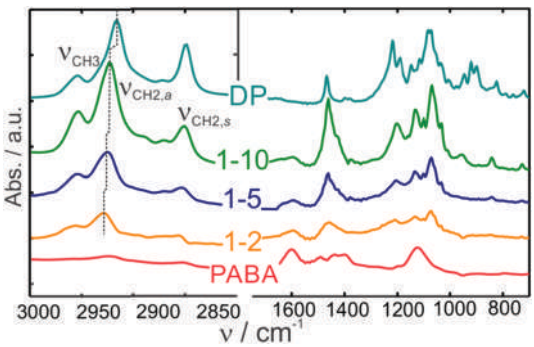

Fig. 2 ATR-FTIR spectra of PABADP and assembled films. Spectra were shifted in absorbance for clarity reasons.

dissimilar film thicknesses. The values of the film thickness determined by spectroscopic ellipsometry are presented in Table 1 (see the ESI†).

In the case of PABA, the band at 1135 cm^{-1} has been assigned to both the aromatic C–H in-plane bending[34,35] and an N═Q═N stretching mode.[34,36] This band is related to another band at 1612 cm^{-1}, which has been assigned to other N═Q═N stretching.[34–37] There are also other less important bands at 1455 cm^{-1}, assigned to aromatic C–C[35] or C–N stretching;[37] and at 1500 cm^{-1}, which has been assigned to N–B–N stretching;[36] or Q═N–B stretching.[37] The characteristics of the IR of PABA suggest that it presents a high degree of oxidized quinone-imine-like units, in accordance with the XPS results.

Some characteristic bands of organic phosphate also appear in the region 800 to 1500 cm^{-1} (Fig. 2 right). The bands at 1030–1090 cm^{-1} have been assigned to P–O stretching modes in POC moieties[38] whereas the bands at about 950 cm^{-1} are due to P–OH stretching modes.[38] Bands at about 1150–1250 cm^{-1} are assigned to P═O stretching.[39] Other bands at 1100–1190 cm^{-1} could be assigned to C–C and C–O stretching and the intense band at 1470 cm^{-1} would be due to HCH scissoring modes.[40] However, the interesting information comes from the 3000 cm^{-1} region arising from C–H stretching (Fig. 2, left). The bands at about 2850 and 2920 cm^{-1} correspond to symmetric and asymmetric stretching modes of methylene groups whereas the band at 2950 cm^{-1} is due to C–H stretching modes of the methyl groups.[41] These methylene bands have been extensively utilized as markers for the degree of disorder of packed aliphatic chains.[42,43] As the chains become more disordered, the methylene bands shift to higher wavenumbers and get wider as a consequence of the increase of gauche conformations.[42–44] This is the trend found for the PABA–DP assembled films as the proportion of DP in the starting solution decreases (Table 1). Furthermore, the relative intensity of the bands of methylene has been also utilized as a measure of order.[45] As the proportion of DP in the spin-coating solution decreases, the relative intensity (asym/sym) increases (reaching a minimum in the case of the solid DP, Table 1), reinforcing the idea of a higher degree of aliphatic disorder in the PADA–DP assembled films formed by complexes obtained from dispersions with a lower proportion of surfactant.

Contact angle

The films were also analyzed by contact angle measurements. The measurements with pure water on PABA–DP 1 : 2, 1 : 5 and 1 : 10 films are reported in Table 1. All systems present a hydrophobic behavior, which increases with the molar ratio of the surfactant in the spin-coating solution. The values of the contact angles for these films suggest that the interaction between the surfactant and the polymer promotes a meso-structural organization where the hydrophobic domains are exposed to the aqueous phase.

Mesostructural organization of the PABA–DP films

XRR

X-Ray Reflectivity (XRR) measurements were carried out in order to study the out-off-plane mesostructural organization of the PABA–surfactant films on silicon(100). Fig. 3(a) shows the X-ray reflectivity data of the 1 : 5 PABA–DP self-assembled film (see also the ESI†). The presence of well-defined equally spaced Bragg peaks in the reflectogram of the PABA–DP films indicates highly oriented lamellar structures.

From the Bragg peak positions of the PABA–DP 1 : 2, 1 : 5 and 1 : 10 a lamellar spacing of 3.58 nm, 3.55 nm and 3.59 nm can be determined respectively. The simplest model to describe a lamellar nanostructure formed by a polyelectrolyte and a surfactant is a microphase-separated structure consisting of an ionic phase containing the polyelectrolyte chains and the ionic head groups of the surfactants and a non-ionic phase containing the hydrophobic moieties such as alkyl chains. The values of the lamellar spacing are similar to others found in the literature.[46] Similar values of the interlamellar spacing of the different films indicate the independence of the surfactant concentration and the order of the film structure. An interesting observation is that the reflectivity diagrams also show co-peaks close to the main Bragg reflections placed at higher

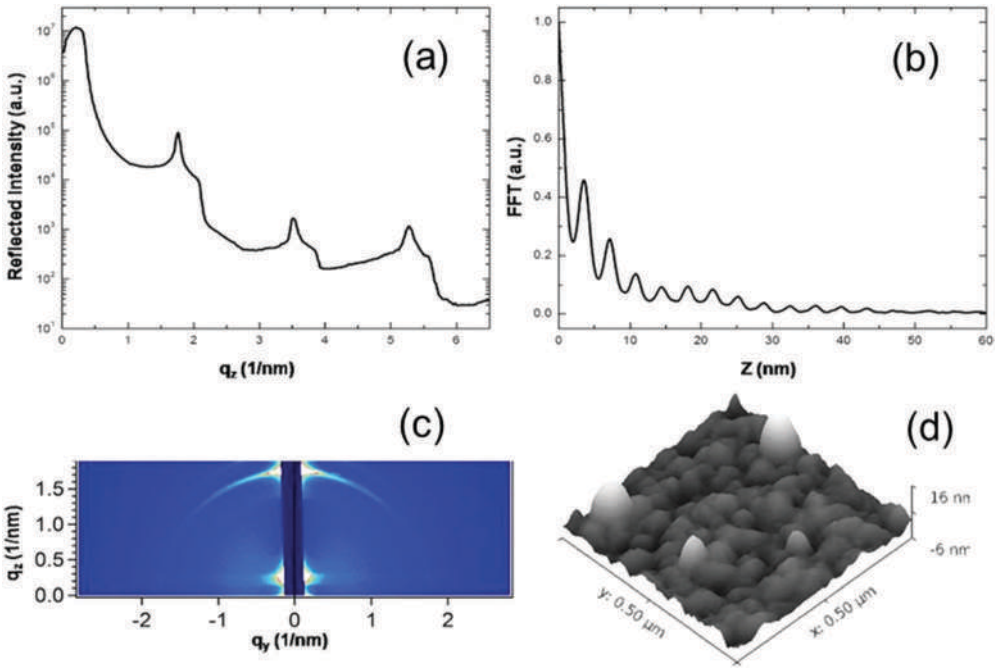

Fig. 3 Structural results obtained for the 1 : 5 PABA–DP film: (a) XRR (b) the FFT of the reflectivity curves (c) GISAXS (d) AFM image.

values of the scattering vector q. From the co-peak positions of the PABA–DP 1 : 2, 1 : 5 and 1 : 10 a lamellar spacing of 3.27 nm, 3.30 nm and 3.26 nm can be determined respectively for the partner phase. The smaller lamellar spacing and the fact that the intensity relation of the co-peak and the main peak is more important at higher surfactant concentrations strongly suggest that the companion phase might be formed by the surfactant. The difference between the values of the lamellar spacing with and without polyelectrolyte gives an estimate of the width that occupies PABA in the lamella. The average value of just 0.28 nm indicates that PABA chains are placed almost perpendicular to the axis defined by the surfactant chains, parallel to the lamellar plane.

Full thickness of the films was obtained by the analysis of the Fourier transformation of the XRR reflectivity curves provided by Bridou *et al.*[47] The Fourier transformation curves (Fig. 3(b)) show a series of peaks that are equidistantly separated with a decay of the intensity of the peaks. The distance between the peaks has an average of 3.26 nm corresponding to the distance obtained for the interlamellar spacing. The number of lamella stacked in each film (and hence, the thickness of the film) can be obtained as the limit when the peak intensity reaches the noise level in the Fourier transformed curve. For the PABA–DP 1 : 10 film 13 peaks and a film thickness of 43 nm can be obtained, for PABA–DP 1 : 5, 8 peaks and a film thickness of 32 nm can be obtained whereas for the PABA–DP 1 : 2 film only 2 not so well defined peaks and a thickness of approximately 10 nm can be deduced in reasonable agreement with thickness values determined by ellipsometry (Table 1). The increasing concentration of DP increases the thickness of the film deposited by spin-coating, allowing us to tune the thickness of the film obtained by changing the concentration of the surfactant used to precipitate it.

The films were also studied using AFM in order to obtain information of the topography. For all films, the AFM images show that the surfaces are smooth with a surface roughness not higher than two stacked lamellas (Fig. 3(d)), indicating that films are mainly homogeneous.

GISAXS

GISAXS experiments were performed with an incident angle of 0.21° to maximize the signal arising from the film (Fig. 3(c)). The GISAXS patterns obtained for the PABA–DP 1 : 2, PABA–DP 1 : 5 and PABA–DP 1 : 10 films show the presence of intense bright spots placed along the q_z direction indicating that the lamellar structures of these films are mainly oriented in a direction parallel to the substrate (see the ESI,† Fig. S5). A halo starting from the q_z direction is also noticeable whose intensity increases with the amount of DP surfactant. The presence of the halo indicates that the lamellar domains, although mainly oriented parallel to the substrate, have an increasing degree of misorientation.

WAXS

The PABA–surfactant complexes dissolved in DMF were deposited on a Mylar substrate to obtain information about the order at an atomic length scale by WAXS (see the ESI,† Fig. S6). It was suggested that Bragg peaks in the region around 15 nm^{-1} should be representative of the lateral order of aliphatic chains.[48–50] The results showed the absence of sharp reflection peaks in the region between 14 nm^{-1} and 18 nm^{-1} indicating the absence of crystalline regions within the films.

Electrochemical response of PABA–DP self-assembled films

This study was carried out to explore the electrochemical response of the PABA–DP complexes. The films were spin-coated over Au substrates in order to obtain PABA–DP-modified electrodes, using the same conditions as those used on the Si substrates. The molar relationships between PABA and DP were the same as those used on the Si substrates: 1 : 2, 1 : 5 and 1 : 10. The voltammetric behavior was first studied in acidic solutions of 0.5 M H_2SO_4, as this kind of PANI-like CPs presents a better electrochemical response under highly acidic conditions.[24]

The voltammograms in acidic solution show a main redox couple at about 0.43 V, in excellent agreement with that reported for electrochemically synthesized PABA in this medium (Fig. 4).[24] The electrochemical response was higher (higher currents) for a lower content of DP in the assembling solution, but it was stable to potential cycling in all cases (Fig. S7, ESI†). These results indicate that PABA remains electroactive within the assemblies with this highly hydrophobic non-electroactive counterpart. As the electron transfer across the films need not only electron propagation but also ionic transport to keep the local electroneutrality, the structure of the assemblies must allow some kind of ionic movement. Charge neutralization could be performed by counterions or co-ions. In the case of PANI-like materials, the oxidation of the totally reduced form (leucoemeraldine to emeraldine) occurs by taking 2 electrons every 4 monomeric units. The positively generated charge in the polymer chains could be compensated by the entrance of anions from solution to the film (the general situation in highly permeable films) or by the proton expulsion from the film (or even more generally, by a combination of these two processes).[51] During reduction (cathodic wave of the voltammograms), the opposite process would take place. Taking into account the general picture of the film mesostructure inferred from the X-ray characterization, proton mobility seems to be much more feasible than anion ingress–egress during the potential scans.

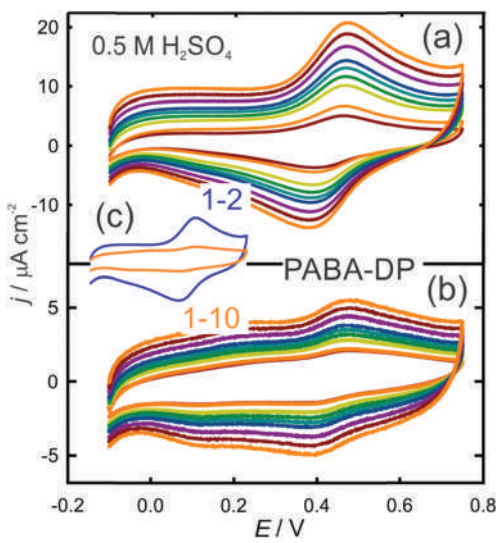

Fig. 4 Voltammetric response of a PABA–DP-coated gold electrode at different sweep rates from 10 to 120 mV s^{-1} in sulfuric acid solution. (a) PABA–DP 1 : 2, (b) PABA–DP 1 : 10. (c) Comparison of the voltammograms for both electrodes at the same scale.

Proton conductivity is responsible for the charge transport in hydrophobic membranes[52] and even proton transport would be enhanced in the present case by using weak polyelectrolytes. Actually, it was shown that 4-aminobenzylamine and phosphate blends can be combined with PSS to yield solid membranes that render high protonic conductivity under water-free conditions.[53] In that case, the temperature dependence of the conductivity suggests that charge transfer is carried out by proton-hopping across the membranes.[53]

Independently of the charge transport mechanism, the higher lamellar order parallel to the electrode surface of the assemblies prepared from solutions with a higher proportion of surfactant evidently hinders charge movement across the film, lowering the net voltammetric current (Fig. 4), as already observed in other mesostructured electroactive systems.[54]

PANI shows an excellent electroactivity in highly acidic solutions, but it rapidly decreases as the pH of the solutions shift to neutral. In contrast to PANI, PABA has been reported to show an appreciably good electroactivity in neutral solution, both when copolymerized with a low proportion of aniline[24] as well as when assembled LbL with anionic polyelectrolytes.[23] The interest for the electroactivity at about pH 7 comes from the potential of these systems to be utilized as redox platforms in bioelectronic devices, as the biochemical components (proteins, aptamers, and enzymes) are naturally designed to operate efficiently at physiological pH. So, the electroactivity of the PABA–DP-modified electrodes was also evaluated in buffer-free 0.1 M KCl (pH 6.5) by cyclic voltammetry. Fig. 5 shows the voltammograms for the 1 : 10 film. Similar results were obtained for the other proportions. The voltammograms obtained showed a linear relationship between the peak current and the sweep rate, which correspond to the electron transfer of a surface-confined redox couple (Fig. 5).[55] The main redox couple clearly shifts to about 0.2 V as previously reported for similar systems.[24] Independently of the proportion of DP in the assembling solutions, all the film-modified electrodes presented similar values of voltammetric current, lower than in acidic solution. However, they all presented a stable redox response, which indicates that the polymer remains electroactive in the environment provided by the surfactant even at neutral pH.

The electrochemical behavior in neutral solution was further studied by evaluating the ability to mediate the electron transfer to an external redox couple. $Fe(CN)_6^{4-/3-}$ was utilized as a model of an electrochemical partner as its electrochemical behavior is well-known and its redox potential is about that of the main couple on the PABA assemblies in 0.1 M KCl (Fig. 6). The results show that the three films prepared, independently of the amount of surfactant used, have a similar ability to transfer electrons to (and from) the redox couple. The systems have a quasi-reversible response.[55] However, the voltammetric current is about 10% of that obtained on a clean

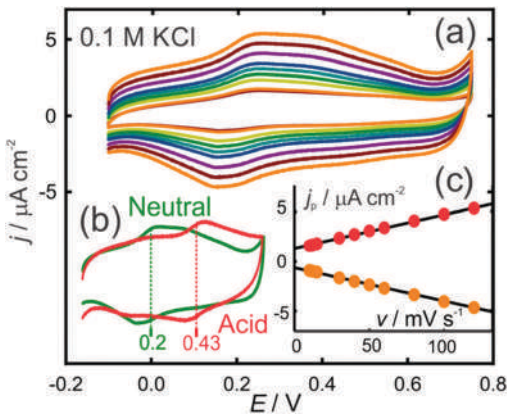

Fig. 5 (a) Voltammetric response of a PABA–DP (1 : 10)-coated gold electrode at different sweep rates from 10 to 120 mV s^{-1} in 0.1 M KCl solution (pH: 6.5) (b) comparison of the voltammograms in 0.1 M KCl and 0.5 M H_2SO_4 for the same electrode at 100 mV s^{-1}. (c) Linear dependence of the voltammetric peak current density on the sweep rate for data in (a).

Au electrode. The reasons for that could be that the effective area for the $Fe(CN)_6^{4-/3-}$ electron transfer is significantly lower or the electron transfer on the surface is much slower. The dependence of the voltammetric current on the sweep rate indicates that the global charge transfer process is limited by semi-infinite diffusion of the redox couple in the solution (Fig. 6).[55] This suggests that the lower current density observed on the PABA–DP films compared with gold is due to a lower electroactive area. This is consistent with the presence of small electroactive polymer domains exposed in the surface of the films. The high contact angle values support this idea, as they indicate that the surface is mainly hydrophobic, suggesting the presence of large patches in which the surfactant tails are exposed to the solution. The similarity of the voltammetric responses in neutral solution in the absence of a redox couple for the different films also suggest that the effectively connected fraction of an electroactive material would be involved in the charge transport to the redox probe as they all yield the same voltammetric currents in the $Fe(CN)_6^{4-/3-}$ solution (Fig. 6).

Of course, the presence of uncoated regions could also explain this fact. Although the films observed by AFM seem to be homogeneous, the presence of pinholes cannot be discarded from the structural characterization. To evaluate the effect of the possible uncoated regions or pinholes, the under potential deposition (UPD) of Cu(II) on both clean and modified gold electrodes was carried out (ESI†).[56] The electrodes were exposed to a 0.06 mM copper sulfate solution in 0.5 M H_2SO_4 and linear sweep voltammetry was performed scanning the potential in the cathodic direction up to a limit value higher than that required for the massive deposition of Cu. Then, the scan was reversed to the initial potential value. The integrated voltammetric charge of the anodic peak due to the redissolution of the deposited Cu measured on the PABA–DP modified electrodes was compared to the value obtained for uncoated gold for estimating the fraction of metal accessible for the deposition. The results show that more than 95% of the surface is blocked for Cu deposition, so the presence of exposed metal regions could be practically discarded, reinforcing the notion that electron transfer takes place at the surface of the self-assembled films.

The characterization obtained by the X-ray techniques shows that the increase of the molar ratio of the surfactant allows for obtaining films thicker and with a better alignment of the polyelectrolyte parallel to the substrate. Those effects should work simultaneously to inhibit the capacity of the system to transfer electrons. In the films the component responsible for transferring electrons is the conducting polymer PABA whereas the intercalated DP in the middle of the polyelectrolyte chains should restrain the capacity to transfer electrons. The lamellar structure obtained from the combination of these components should neglect the connectivity between the chains and this effect should increase with the number of layers. However as the system gets thicker and more ordered, it keeps its electroactivity. To account for this, the lamellas obtained should be visualized not as infinite layers that occupy the whole surface area of the substrate, but as if they are formed by micro lamellas. These micro-domains might have imperfections and edge effects where a certain number of polymer chains can end up making connections between the different layers of PABA. These connections between different polymer layers are responsible for maintaining the conducting properties of the stacked films.

Conclusions

In this work we have prepared polyelectrolyte–surfactant complexes with different relations of surfactant and polymer.

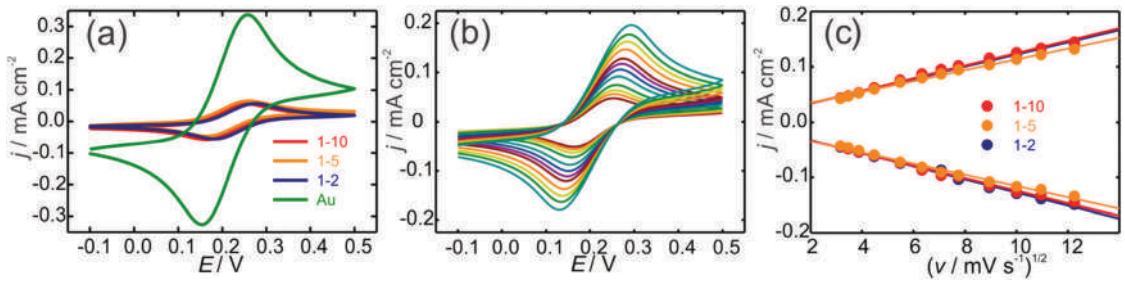

Fig. 6 (a) Comparison of voltammograms for different films and bare gold at 12 mV s^{-1}. (b) Cyclic voltammograms for the PABA–DP 1 : 10-covered electrode at different sweep rates from 10 to 150 mV s^{-1}. (c) Representation of the voltammetric peak current density as a function of the square of the sweep rate for the different films. Conditions: 4 mM $Fe(CN)_6^{4-/3-}$ in 0.1 M KCl, pH 6.5.

After spin-coating, the films presented a well-defined lamellar structure, directed by the strong interaction between the phosphate groups of DP and the positively charged ammonium groups in the polyelectrolyte. The amounts of surfactant used to precipitate the electroactive polymer allowed for obtaining different film thicknesses between 10 and 45 nm. Also, as proven by GISAXS, the proportion of surfactant works as a driving force to order the lamellas parallel to the substrate.

The films obtained displayed intrinsic electroactivity in both acidic and neutral solutions. The self-assembled films were also able to manage the electron transfer to a soluble reversible redox couple. These results suggest that although the increment of the surfactant concentration yields more ordered stratified and hydrophobic coatings, the PANI-like polymer remains electroactive and ionic transport is still possible through the film.

The enhanced electroactivity in a neutral solution of PABA as compared with PANI also makes these assembled films good platforms for the integration of bioelectroactive proteins, such as glucose oxidase. Furthermore, due to their high hydrophobicity, they could also provide an adequate environment for membrane or membrane-associated proteins, which may pave the way to new bio-nanoarchitectonic devices.

The presented results also open the door to further studies involving assemblies of PABA and other surfactants in order to enhance their conducting properties for the design of highly connected films as electroactive components in sensing or energy devices.

Conflicts of interest

There are no conflicts to declare.

Acknowledgements

The authors acknowledge financial support from ANPCyT (PICT-2013-0905 and PICT-2015-0239), Universidad Nacional de La Plata (PPID-X016), and the Marie Curie project ''Hierarchical functionalization and assembly of Graphene for multiple device fabrication'' (HiGRAPHEN) (Grant ref. 612704). A. L. thanks a fellowship from CONICET. W. A. M., M. C. and O. A. are CONICET staff members.

Notes and references

1 C. F. J. Faul, *Acc. Chem. Res.*, 2014, **47**, 3428–3438.
2 C. K. Ober and G. Wegner, *Adv. Mater.*, 1997, **9**, 17–31.
3 M. Aono and K. Ariga, *Adv. Mater.*, 2016, **28**, 989–992.
4 K. Ariga, Q. Ji, W. Nakanishi, J. P. Hill and M. Aono, *Mater. Horiz.*, 2015, **2**, 406–413.
5 K. Ariga, Y. Yamauchi and M. Aono, *APL Mater.*, 2015, **3**, 61001.
6 J. Kim, J. H. Kim and K. Ariga, *Joule*, 2017, 1–30.
7 G. Inzelt, *J. Solid State Electrochem.*, 2011, **15**, 1711–1718.
8 G. Inzelt, *Conducting Polymers: A New Era in Electrochemistry*, Springer-Verlag, Berlin Heidelberg, 2nd edn, 2012.
9 J. Heinze, B. A. Frontana-Uribe and S. Ludwigs, *Chem. Rev.*, 2010, **110**, 4724–4771.
10 L. Chen, S. Xu, D. McBranch and D. Whitten, *J. Am. Chem. Soc.*, 2000, **122**, 9302–9303.
11 A. H. Khan, S. Ghosh, B. Pradhan, A. Dalui, L. K. Shrestha, S. Acharya and K. Ariga, *Bull. Chem. Soc. Jpn.*, 2017, **90**, 627–648.
12 J. Kim, J. H. Kim and K. Ariga, *Joule*, 2017, **1**, 739–768.
13 G. Ćirić-Marjanović, *Synth. Met.*, 2013, **170**, 31–56.
14 J. Stejskal, M. Trchová, P. Bober, P. Humpolíček, V. Kašpárková, I. Sapurina, M. A. Shishov and M. Varga, *Encyclopedia of Polymer Science and Technology*, John Wiley & Sons, Inc., 2015.
15 W. A. Marmisollé and O. Azzaroni, *Nanoscale*, 2016, **8**, 9890–9918.
16 D. S. Sutar, N. Padma, D. K. Aswal, S. K. Deshpande, S. K. Gupta and J. V. Yakhmi, *Sens. Actuators, B*, 2007, **128**, 286–292.
17 D. S. Sutar, N. Padma, D. K. Aswal, S. K. Deshpande, S. K. Gupta and J. V. Yakhmi, *J. Colloid Interface Sci.*, 2007, **313**, 353–358.
18 H. Kosonen, J. Ruokolainen, M. Knaapila, M. Torkkeli, K. Jokela, R. Serimaa, G. Ten Brinke, W. Bras, A. P. Monkman and O. Ikkala, *Macromolecules*, 2000, **33**, 8671–8675.
19 A. D. W. Carswell, E. A. O'Rea and B. P. Grady, *J. Am. Chem. Soc.*, 2003, **125**, 14793–14800.
20 J. Ruiz, B. Gonzalo, J. R. Dios, J. M. Laza, J. L. Vilas and L. M. León, *Adv. Polym. Technol.*, 2013, **32**, E180–E188.
21 T. G. Dane, P. T. Cresswell, G. A. Pilkington, S. Lilliu, J. E. Macdonald, S. W. Prescott, O. Bikondoa, C. F. J. Faul and W. H. Briscoe, *Soft Matter*, 2013, **9**, 10501.
22 T. G. Dane, P. T. Cresswell, O. Bikondoa, G. E. Newby, T. Arnold, C. F. J. Faul and W. H. Briscoe, *Soft Matter*, 2012, **8**, 2824–2832.
23 W. A. Marmisollé, E. Maza, S. Moya and O. Azzaroni, *Electrochim. Acta*, 2016, **210**, 435–444.
24 W. A. Marmisollé, D. Gregurec, S. Moya and O. Azzaroni, *ChemElectroChem*, 2015, **2**, 2011–2019.
25 N. Kröger, S. Lorenz, E. Brunner and M. Sumper, *Science*, 2002, **298**, 584–586.
26 N. Kröger, R. Deutzmann, C. Bergsdorf and M. Sumper, *Proc. Natl. Acad. Sci. U. S. A.*, 2000, **97**, 14133–14138.
27 L. D'Agostino and A. Di Luccia, *Eur. J. Biochem.*, 2002, **269**, 4317–4325.
28 L. D'Agostino, M. di Pietro and A. Di Luccia, *FEBS J.*, 2005, **272**, 3777–3787.
29 W. A. Marmisollé, J. Irigoyen, D. Gregurec, S. Moya and O. Azzaroni, *Adv. Funct. Mater.*, 2015, **25**, 4144–4152.
30 W. J. Dressick, K. J. Wahl, N. D. Bassim, R. M. Stroud and D. Y. Petrovykh, *Langmuir*, 2012, **28**, 15831–15843.
31 G. Laucirica, W. A. Marmisollé and O. Azzaroni, *Phys. Chem. Chem. Phys.*, 2017, **19**, 8612–8620.
32 P. N. Bartlett and E. N. K. Wallace, *Phys. Chem. Chem. Phys.*, 2001, **3**, 1491–1496.
33 A. M. Bonastre, M. Sosna and P. N. Bartlett, *Phys. Chem. Chem. Phys.*, 2011, **13**, 5365–5372.

34 J. Laska and J. Widlarz, *Polymer*, 2005, **46**, 1485–1495.
35 C. Sanchís, H. J. Salavagione, J. Arias-Pardilla and E. Morallón, *Electrochim. Acta*, 2007, **52**, 2978–2986.
36 J. Tang, X. Jing, B. Wang and F. Wang, *Synth. Met.*, 1988, **24**, 231–238.
37 Y. Furukawa, F. Ueda, Y. Hyodo, I. Harada, T. Nakajima and T. Kawagoe, *Macromolecules*, 1988, **21**, 1297–1305.
38 J. O. Carnali and B. A. Pethica, *J. Phys. Chem. B*, 2006, **110**, 24936–24946.
39 I. Maege, E. Jaehne, A. Henke, H.-J. P. Adler, C. Bram, C. Jung and M. Stratmann, *Prog. Org. Coat.*, 1998, **34**, 1–12.
40 A. N. M. Carauta, V. De Souza, E. Hollauer and S. C. A. Téllez, *Spectrochim. Acta, Part A*, 2004, **60**, 41–51.
41 R. MacPhail, H. Strauss, R. Snyder and C. Elliger, *J. Phys. Chem.*, 1984, **88**, 334–341.
42 R. A. Vaia, R. K. Teukolsky and E. P. Giannelis, *Chem. Mater.*, 1994, **6**, 1017–1022.
43 W. Wang, L. Li and S. Xi, *J. Colloid Interface Sci.*, 1993, **155**, 369–373.
44 T. Kawai, J. Umemura, T. Takenaka, M. Kodama and S. Seki, *J. Colloid Interface Sci.*, 1985, **103**, 56–61.
45 R. G. Snyder, H. L. Strauss and C. A. Elliger, *J. Phys. Chem.*, 1982, **86**, 5145–5150.
46 M. L. Cortez, G. A. González, M. Ceolín, O. Azzaroni and F. Battaglini, *Electrochim. Acta*, 2014, **118**, 124–129.
47 F. Bridou and B. Pardo, *J. X-Ray Sci. Technol.*, 1994, **4**, 200–216.
48 D. M. Small, *J. Lipid Res.*, 1984, **25**, 1490–1500.
49 D. Marsh, *Chem. Phys. Lipids*, 2012, **165**, 59–76.
50 D. Marsh, *Handbook of Lipid Bilayers*, CRC Press, Boca Raton, 2nd edn, 2013.
51 W. A. Marmisollé, M. I. Florit and D. Posadas, *J. Electroanal. Chem.*, 2014, **734**, 10–17.
52 K. D. Kreuer, *J. Membr. Sci.*, 2001, **185**, 29–39.
53 J. Jalili and V. Tricoli, *Front. Energy Res.*, 2014, **2**, 1–5.
54 M. Lorena Cortez, N. De Matteis, M. Ceolín, W. Knoll, F. Battaglini and O. Azzaroni, *Phys. Chem. Chem. Phys.*, 2014, **16**, 20844–20855.
55 A. J. Bard and L. R. Faulkner, *Electrochemical Methods. Fundamentals and Applications*, USA, 2nd edn, 2001.
56 M. C. Santos, L. H. Mascaro and S. A. S. Machado, *Electrochim. Acta*, 1998, **43**, 2263–2272.

